

Exclusion limits on Dark Matter-Neutrino Scattering Cross-section

Diptimoy Ghosh,^{1,*} Atanu Guha,^{1,†} and Divya Sachdeva^{1,‡}

¹*Department of Physics, Indian Institute of Science Education and Research Pune, India*

We derive new constraints on combination of dark matter - electron cross-section ($\sigma_{\chi e}$) and dark matter - neutrino cross-section ($\sigma_{\chi\nu}$) utilising the gain in kinetic energy of the dark matter (DM) particles due to scattering with the cosmic ray electrons and the diffuse supernova neutrino background (DSNB). Since the flux of the DSNB neutrinos is comparable to the CR electron flux in the energy range $\sim 1 \text{ MeV} - 50 \text{ MeV}$, scattering with the DSNB neutrinos can also boost low-mass DM significantly in addition to the boost due to interaction with the cosmic ray electrons. We use the XENON1T as well as the Super-Kamiokande data to derive bounds on $\sigma_{\chi e}$ and $\sigma_{\chi\nu}$. While our bounds for $\sigma_{\chi e}$ are comparable with those in the literature, we show that the Super-Kamiokande experiment provides the strongest constraint on $\sigma_{\chi\nu}$ for DM masses below a few MeV.

I. INTRODUCTION

The presence of dark matter (DM) in the universe and its dominance over luminous matter is well-established. DM is known to be non-relativistic and very weakly interacting with the Standard Model (SM) particles. The existence of DM has been inferred only via their gravitational interactions, and both the DM mass and their exact interaction strengths with the SM particles are unknown (see [1–4] for reviews).

The DM-proton and DM-electron interaction strengths have been constrained severely by various direct detection (DD) experiments [5–9]. Their basic working principle is to measure the recoil energy of electron/nucleus once the incoming DM particles scatter of them. But one major limitation of this method is that these DD experiments lose sensitivity rapidly for low mass DM (below DM mass of $\sim 5 \text{ GeV}$ for DM-proton cross-section [10], and below DM mass of $\sim 5 \text{ MeV}$ for DM-electron cross-section [11]) since very light DM particles cannot produce enough recoil to be detected. The most stringent constraints on DM-electron scattering cross-section comes from the SENSEI experiment: $\sigma_{\chi e} \lesssim 10^{-34} \text{ cm}^2$ for $m_\chi > 5 \text{ MeV}$ [12].

In the past few decades many other novel detection strategies have been developed: employing the energy deposition in white dwarfs or neutron stars [13–22], from Big Bang Nucleosynthesis [23–25], DM production in astrophysical objects [26], cooling of stars and supernovae [27–31], colliders searches etc. [32, 33]. Cosmological observations have also been used to constrain interactions of low mass DM [34, 35]. For example, CMB spectral distortion excludes DM-electron scattering cross-section above $\sigma_{\chi e} \sim 10^{-28} \text{ cm}^2$ for $m_\chi \lesssim 0.1 \text{ MeV}$ [34] if the cross section is momentum independent.

The DM-neutrino cross-section ($\sigma_{\chi\nu}$), which is the focus of our study, cannot be independently constrained by the DD experiments since matter is not made of neu-

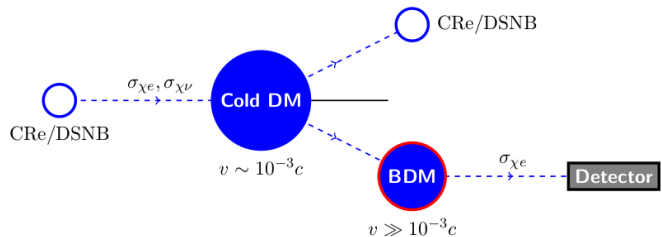


FIG. 1. Schematic diagram for production of boosted dark matter (BDM) due to scattering with CR electrons (CRE) and DSNB neutrinos, and their subsequent detection at the detectors.

trinos. However, as we will discuss later, the DD experiments can be used to constrain a function of $\sigma_{\chi\nu}$ and $\sigma_{\chi e}$ (for more details refer to Sec. IV). Independent bound on $\sigma_{\chi\nu}$ does however exist from Planck and large scale structure experiments: $\sigma_{\chi\nu} \lesssim 10^{-33} (m_\chi/\text{GeV}) \text{ cm}^2$ if the cross section is momentum independent [36].

In order to recover the sensitivity of the DD experiments for low mass DM, the idea of Boosted Dark Matter (BDM) has been explored in recent years. In this scenario, the DM is boosted to higher velocity due to scattering with various cosmic ray components (see Fig. 1 for a schematic diagram) This idea has been explored using CR protons [37–39], helium nuclei [37], cosmic electrons [38–43], and neutrinos from various astrophysical sources [44–48].

Our Universe is abundant in MeV energy neutrinos emerging from massive stars going supernova, right from the epoch of first star formation. Similarly, our galaxy also has energetic electron flux. We consider that the DM in the Milky Way halo experiences scattering with the DSNB neutrinos as well as the cosmic electrons, and gets boosted to velocities $v \gg 10^{-3}c$. Such upscattered low-mass DM can leave interesting signatures in low-energy recoil experiments like XENON1T (where detectable electron recoil energies are of the order of few keV because it is based on the scintillation process), as well as in high-energy recoil experiments like Super-Kamiokande (where detectable electron recoil energies are of the order of few MeV because Super-K relies on

* diptimoy.ghosh@iiserpune.ac.in

† atanu.guha@students.iiserpune.ac.in

‡ divya.sachdeva@students.iiserpune.ac.in

Cherenkov radiation).

In earlier studies, CR electrons and DSNB were separately considered as the particles transferring kinetic energy to the DM. However, as shown in Fig. 2, the fluxes for CR electrons and DSNB neutrinos are comparable in the energy range $1 \text{ MeV} \lesssim T_i \lesssim 50 \text{ MeV}$ motivating us to include both these contributions to the DM boost. Note that, while studying $\sigma_{\chi e}$, $\sigma_{\chi\nu}$ can in principle be set to zero but the vice versa cannot be done since, for the detection of the DM signal, the existence of $\sigma_{\chi e}$ is crucial. And once $\sigma_{\chi e}$ is non-zero, it will also contribute to boost the DM and must be taken into account in a consistent analysis. In this work, we have thus taken into account contributions to the DM boost due to the CR electrons as well as the DSNB neutrinos, and used the XENON1T [6] and Super-Kamiokande [49] data to provide exclusion limit on the DM-neutrino and DM-electron interactions. To our knowledge, we are the first to use the Super-Kamiokande data to constrain the

DM-neutrino cross-section, and we show that it provides the strongest direction detection bound in the DM mass range below $\sim 10 \text{ MeV}$.

The paper is organized as follows. In Sec. II, we discuss the DSNB and cosmic ray electron flux as a function of energy. In Sec. III, we calculate the flux of boosted dark matter which is used to calculate rate of scattering (Sec. IV) in different detectors. This rate is then compared and analyzed with the observations of Xenon1T and Super Kamiokande using χ^2 statistics in section V. In Sec. VI, we discuss our results and conclude.

II. COSMIC RAY ELECTRON AND NEUTRINO FLUX

CR electron flux can be described by certain parameterization of the local interstellar spectrum [50] given as

$$F(T_e) = \begin{cases} \frac{1.799 \times 10^{44} T_e^{-12.061}}{1 + 2.762 \times 10^{36} T_e^{-9.269} + 3.853 \times 10^{40} T_e^{-10.697}} & \text{if } T_e < 6880 \text{ MeV} \\ 3.259 \times 10^{10} T_e^{-3.505} + 3.204 \times 10^5 T_e^{-2.620} & \text{if } T_e \geq 6880 \text{ MeV} \end{cases} \quad (1)$$

where the unit of $F(T_e)$ is given in $(\text{m}^2 \text{ s sr MeV})^{-1}$ and the kinetic energy (T_e) of the CR electrons is in MeV. The above parameterization is in accordance with Fermi-LAT [51–54], AMS-02 [55], PAMELA [56, 57], and Voyager [58, 59] data.

On the other hand, the DSNB flux can be calculated from the knowledge of the rate of core-collapse supernovae (R_{CCSN}) [60, 61]

$$\Phi_\nu(E_\nu) \Big|_{DSNB} = \int_0^{z_{max}} \frac{dz}{H(z)} R_{CCSN}(z) F_\nu(E'_\nu) \quad (2)$$

The R_{CCSN} is a function of star formation rate and has been calculated following [62]. The observable effective spectra of the neutrinos emitted from supernovae, is assumed to be of Fermi-Dirac form and approximately given for each flavour as [60, 62]

$$F_\nu(E_\nu) = \frac{E_\nu^{tot}}{6} \frac{120 E_\nu^2}{7\pi^4 T_\nu^4} \frac{1}{\exp(\frac{E_\nu}{T_\nu}) + 1} \quad (3)$$

where $E_\nu^{tot} \approx 5 \times 10^{52} \text{ erg}$ is the total energy released in the supernova explosion in the form of neutrinos. T_ν is the temperature of the neutrinos. Supernova simulations and Super-Kamiokande observations suggest the estimates of the temperatures to be $T_\nu = 4 \text{ MeV}$ for ν_e , $T_\nu = 5 \text{ MeV}$ for $\bar{\nu}_e$ and $T_\nu = 8 \text{ MeV}$ for $\nu_\mu, \bar{\nu}_\mu, \nu_\tau, \bar{\nu}_\tau$ [62, 63]. $E'_\nu = E_\nu(1+z)$ is the observed

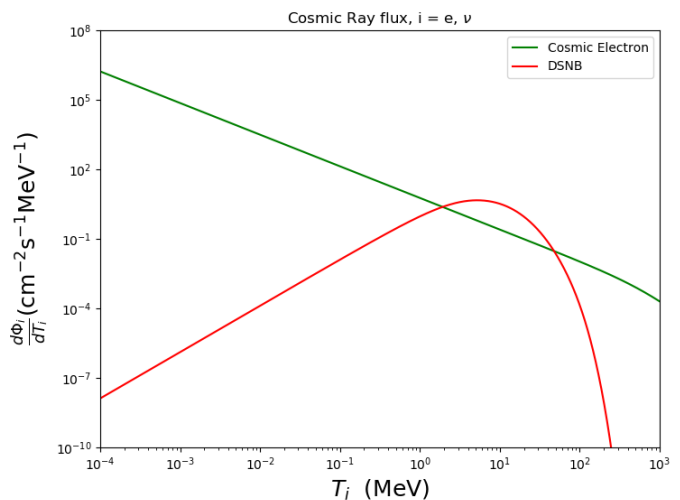


FIG. 2. Fluxes of cosmic ray electrons and the diffuse supernova neutrino background (summing over all flavours of neutrinos).

energy at earth due to redshift z . The maximum redshift is generally taken to be $z_{max} = 5$. The Hubble function is given by $H(z) = H_0 \sqrt{\Omega_\Lambda + \Omega_m(1+z)^3}$, where, $H_0 = 67 \text{ kms}^{-1} \text{ Mpc}^{-1}$. $\Omega_\Lambda = 0.7$ and $\Omega_m = 0.3$ are the vacuum and matter contribution to the energy density of the Universe, respectively [64].

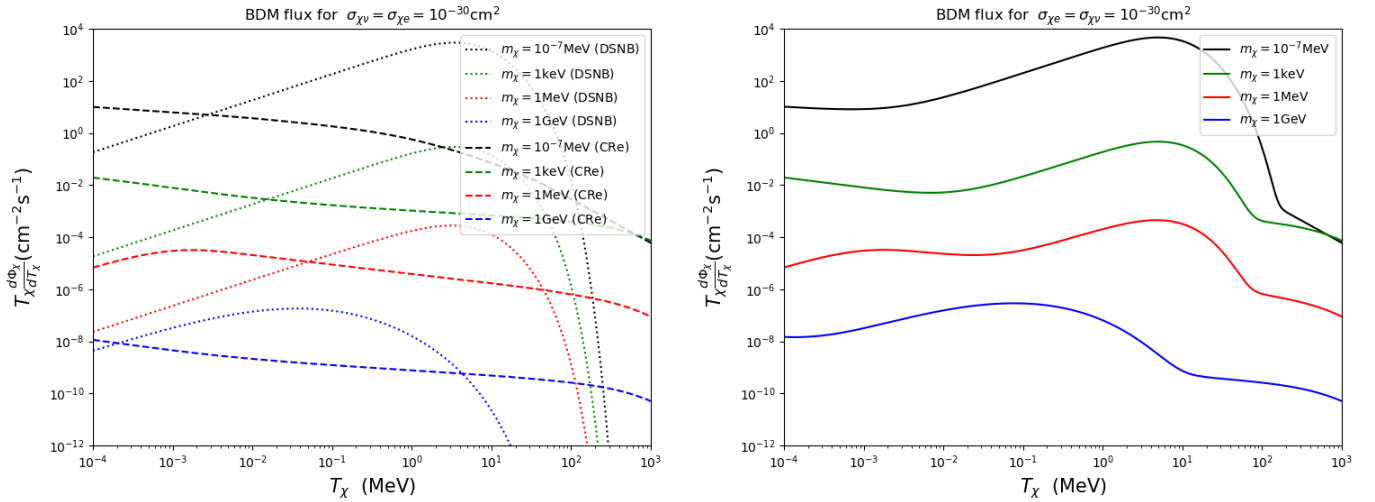


FIG. 3. CR electrons and DSNB induced BDM flux for $\sigma_{\chi e} = \sigma_{\chi \nu} = 10^{-30} \text{ cm}^2$. The left panel shows the BDM flux due to the individual boost by CR electrons (dashed lines) and DSNB neutrinos (dotted lines). The right panel shows the BDM flux due to the combined effect.

Fig. 2 shows the cosmic ray electron flux along with the flux of neutrinos coming from supernovae. As can be observed from this figure, for $1 \text{ MeV} < T_i < 50 \text{ MeV}$, both the fluxes are of similar order and this range is crucial for boosting DM with mass below MeV. This fact inspire us to consider both the fluxes to derive bounds on $\sigma_{\chi \nu}$ and $\sigma_{\chi e}$ for light DM case considered here.

III. BOOSTED DARK MATTER FLUX

Cold dark matter (DM) particles get boosted after getting hit by cosmic ray electrons and DSNB. We calculated the flux of the boosted DM using the cosmic ray electron and neutrino fluxes discussed at Sec. II following [37, 38, 40].

For i -DM scattering ($i = e, \nu$), the energy transfer to the cold DM by the CR electron/DSNB is given by

$$T_\chi = T_\chi^{max} \left(\frac{1 - \cos \theta}{2} \right)$$

$$T_\chi^{max} = \frac{(T_i)^2 + 2T_i m_i}{T_i + (m_i + m_\chi)^2 / (2m_\chi)} \quad (4)$$

where θ is the scattering angle at the centre of momentum frame.

Solving Eq. 4 we get the minimum required energy of the electrons/neutrinos to produce a certain amount of kinetic energy of the boosted DM

$$T_i^{min} = \left(\frac{T_\chi}{2} - m_i \right) \left[1 \pm \sqrt{1 + \frac{2T_\chi (m_i + m_\chi)^2}{m_\chi (2m_i - T_\chi)^2}} \right] \quad (5)$$

The + and - sign in Eq. (5) are applicable for $T_\chi > 2m_i$ and $T_\chi < 2m_i$, respectively.

For the elastic scattering cross-section $\sigma_{\chi i}$, the collision rate of i - χ per unit volume, having kinetic energy of the particle i in the range $[T_i, T_i + dT_i]$, is given by

$$\frac{d\Gamma}{dV} = \sigma_{\chi i} \times n_\chi \times d\Phi_i$$

$$d\Gamma = \sigma_{\chi i} \times \frac{\rho_\chi}{m_\chi} \times \frac{d\Phi_i}{dT_i} dT_i dV \quad (6)$$

Where, $\frac{d\Phi_i}{dT_i}$ is the Local Interstellar Spectrum for the particle i . The solid angle subtended by a small facet having flat surface area ds , orientation \hat{n} and distance d from the viewer is

$$d\Omega = 4\pi \left(\frac{ds}{4\pi d^2} \right) (\hat{d} \cdot \hat{n}) \quad (7)$$

If d is very large, $\hat{d} \cdot \hat{n} \approx 1$.

We consider that the incoming electrons/neutrinos with kinetic energy $[T_i, T_i + dT_i]$ are contained within dV . Let dl be the length at which dV is spread along $\hat{d} \approx \hat{n}$ and $ds\hat{n}$ be the area vector of the flat surface. In that case, $dV \approx dl \cdot ds$ and $4\pi d^2$ is the area of the sphere of radius d around the DM particles.

Electrons/neutrinos are going out from dV to all direction. But we are interested only those who are directed towards the DM. Therefore, i induced DM flux is given by

$$\frac{d\Phi_\chi}{dT_i} = \int \sigma_{\chi i} \cdot \frac{\rho_\chi}{m_\chi} \cdot \frac{d\Phi_i}{dT_i} \cdot dl \cdot \frac{ds}{4\pi d^2}$$

$$= \int_{\text{Line of sight}} \sigma_{\chi i} \cdot \frac{\rho_\chi}{m_\chi} \cdot \frac{d\Phi_i}{dT_i} \cdot dl \cdot \frac{d\Omega}{4\pi} \quad (8)$$

Now we have to integrate over all possible line segment dl along the line of sight. Let D_{eff} be the effective distance out to which all the electrons/neutrinos have to be

taken into account. So, for homogeneous and isotropic distribution of DM and i

$$\frac{d\Phi_\chi}{dT_i} = \sigma_{\chi i} \times \frac{\rho_\chi}{m_\chi} \times \frac{d\Phi_i}{dT_i} \cdot D_{eff} \quad (9)$$

In our present work, we consider the effective distance for the DSNB to be $D_{eff} = 10$ kpc and for the incoming cosmic ray electrons $D_{eff} = 1$ kpc. As an independent variable, if T_χ is having flat distribution (i.e., T_χ can take any value in the range $[0, T_\chi^{max}]$ with equal probability), we can write,

$$\frac{d\Phi_\chi}{dT_\chi} = \frac{\Phi_\chi}{T_\chi^{max}} \Theta(T_\chi^{max} - T_\chi) \quad (10)$$

But Φ_χ and T_χ^{max} both are functions of T_i , and in that case Φ_χ can be written as

$$\Phi_\chi = \int_{T_i=0}^{\infty} d\Phi_\chi(T_i)$$

Thus,

$$\left(\frac{d\Phi_\chi}{dT_\chi}\right)_i = \int_0^{\infty} dT_i \frac{d\Phi_\chi}{dT_i} \frac{1}{T_\chi^{max}(T_i)} \Theta [T_\chi^{max}(T_i) - T_\chi] \quad (11)$$

The heaviside step function $\Theta [T_\chi^{max}(T_i) - T_\chi]$ inside the integration $\int_0^{\infty} dT_i \dots$ ensures that $T_\chi^{max} > T_\chi$, where T_χ is a random variable having a flat distribution. In that way $\Theta [T_\chi^{max}(T_i) - T_\chi]$ turns the above integral to a more meaningful one $\int_{T_i^{min}}^{\infty} \dots$. In other words, the Θ function ensures that T_χ cannot take any value independent of T_i and T_i has a minimum value to produce a particular T_χ . So finally Eq.(11) can be rewritten as

$$\left(\frac{d\Phi_\chi}{dT_\chi}\right)_i = \int_{T_i^{min}}^{\infty} dT_i \frac{d\Phi_\chi}{dT_i} \frac{1}{T_\chi^{max}(T_i)} \quad (12)$$

Putting everything together, we get the following expression for the i -boosted DM flux from Eq.(11)

$$\left(\frac{d\Phi_\chi}{dT_\chi}\right)_i = D_{eff} \times \frac{\rho_\chi^{local}}{m_\chi} \int_{T_i^{min}}^{\infty} dT_i \frac{d\Phi_i}{dT_i} \frac{1}{T_\chi^{max}(T_i)} \quad (13)$$

Using Eq. (13), we obtain the BDM fluxes and show them Fig. 3. The bumps in the right panel of Fig. 3 are due to the behaviour of DSNB spectrum.

IV. RATE EQUATION

Using the BDM flux obtained in Sec. III, Eq. (13), we get the differential recoil rate as follows

$$\frac{dR}{dE_R} = \aleph \sigma_{\chi e} \int_{T_\chi^{min}(E_R)}^{\infty} dT_\chi \sum_{i=e,\nu} \left(\frac{d\Phi_\chi}{dT_\chi}\right)_i \frac{1}{E_R^{max}(T_\chi)} \quad (14)$$

where, $E_R^{max}(T_\chi)$ and $T_\chi^{min}(E_R)$ are obtained using Eqs. (4) and (5) with the simple replacements $i \rightarrow \chi$ and $\chi \rightarrow e$, respectively. As different experiments provide the event rate R in different units, we incorporate this fact in a single expression (Eq. 14) via parameter \aleph . Thus, the recoil spectrum for XENON1T is obtained by taking $\aleph = Z_{Xe}/m_{Xe}$, where Z_{Xe} is atomic number of Xenon and m_{Xe} is the mass of a single Xenon atom. In case of the SK-I data, this factor corresponds to the total number of electrons, $\aleph = 7.5 \times 10^{33}$ [39, 40, 49].

Following Eq.(14) we expand the recoil spectra for XENON1T and Super-Kamiokande to obtain

$$\frac{dR}{dE_R} = A \sigma_{\chi e} \sigma_{\chi \nu} + B \sigma_{\chi e}^2 \quad (15)$$

with

$$A = \aleph D_{eff}^{\nu} \frac{\rho_\chi}{m_\chi} \int_{T_\chi^{min}(E_R)}^{\infty} \frac{dT_\chi}{E_R^{max}(T_\chi)} \int_{T_\nu^{min}}^{\infty} \frac{dT_\nu}{T_\chi^{max}(T_\nu)} \frac{d\Phi_\nu}{dT_\nu} \quad (16)$$

and

$$B = \aleph D_{eff}^e \frac{\rho_\chi}{m_\chi} \int_{T_\chi^{min}(E_R)}^{\infty} \frac{dT_\chi}{E_R^{max}(T_\chi)} \int_{T_e^{min}}^{\infty} \frac{dT_e}{T_\chi^{max}(T_e)} \frac{d\Phi_e}{dT_e} \quad (17)$$

where A and B are functions of DM mass and electron recoil energy. In Appendix A, we show the variations of A and B with respect to the electron recoil energy for different values of m_χ (Fig. 14) and with respect to the DM mass at fixed electron recoil energies (Fig. 15). As it can be noticed from Fig. 14, for sub-MeV DM mass regime, A dominates over B . Thus, the right side of Eq. 15 gets most of the contribution from the A term. This implies, for that mass range, the boost due to the scattering with DSNB neutrinos play the dominant role. This will also be clear in the next section.

V. χ^2 ANALYSIS

To find the best-fit point and the exclusion region, we perform a χ^2 analysis using the following definitions

$$\chi^2 = \sum_i \frac{(O_i - E_i)^2}{E_i + (\sigma_i^2)_{data}} \quad (18)$$

$$\Delta\chi^2 = \chi^2(BDM + B_0) - \chi^2(B_0 \text{ only}) \quad (19)$$

where, O_i are the observed number of events, E_i are the expected number of events and $(\sigma_i)_{data}$ is uncertainty in the measured data. For the $(BDM + B_0)$ case, to calculate the E_i values, we sum the BDM signal and the background B_0 for each energy bin.

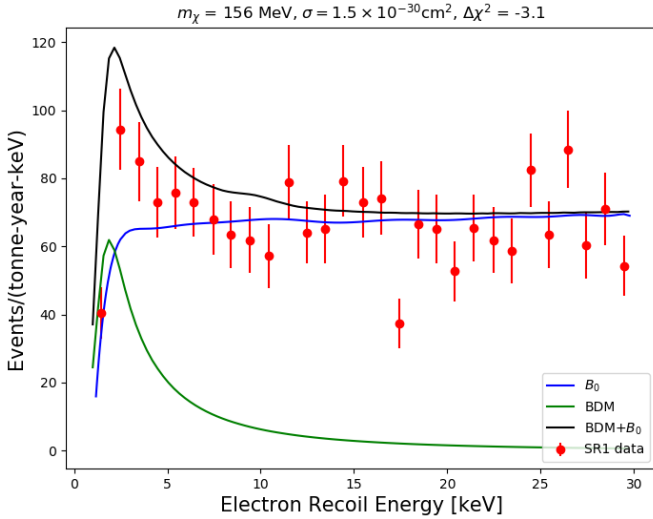


FIG. 4. Scientific Run 1 (SR1) data (in red) along with the estimated background, B_0 (in blue) reported by the XENON collaboration [6]. An example spectrum corresponding to the best-fit point $(m_\chi, \sigma) = (156 \text{ MeV}, 1.5 \times 10^{-30} \text{ cm}^2)$ is also shown (green and black) for DM boosted by CRE and DSNB neutrinos both.

Xenon1T

The XENON1T experiment is operated using a dual-phase liquid-xenon time projection chamber. The detector is capable of producing both prompt scintillation (S1) and delayed electroluminescence (S2) signals. The S2/S1 ratio is further used to distinguish electronic recoils from nuclear recoils. The XENON collaboration, last year, reported a 3.5σ excess of events in the electron recoil range of $1 \text{ keV} < E_R < 7 \text{ keV}$ with 285 events over the backgrounds of 232 ± 15 events. This data was acquired in total 277 days of live-time, which is referred to as Science Run 1 (SR1) [6, 65]. We use this data for the χ^2 analysis to obtain the best-fit point as well as the exclusion region in (m_χ, σ) plane. In Fig. 4, we have shown the SR1 data (in red) along with the predicted background B_0 (in blue). The expected no. of events from boosted DM for the best-fit point along with the corresponding total number of events including the background are also shown.

As it is evident from Fig. 4, the expected background (B_0) can not explain the SR1 data. We estimated $\chi^2(B_0 \text{ only})$ to be ~ 27.1 . Clearly, if the BDM contribution explains SR1 data, $\Delta\chi^2$ must be less than 0 commensurating with a better fit. To derive the exclusion limit with the 95% confidence, we demand $\Delta\chi^2 > 40.1$ that corresponds to 27 degrees of freedom. We present the obtained exclusion region in the $m_\chi - \sigma_{\chi e}$ plane assuming $\sigma_{\chi\nu} = 0$ in Fig. 5. Our results agree very well with the one presented in [42] providing a good cross-check of our analysis. The best-fit point marked with red is given by $(m_\chi, \sigma) = (156 \text{ MeV}, 1.5 \times 10^{-30} \text{ cm}^2)$ corresponding to

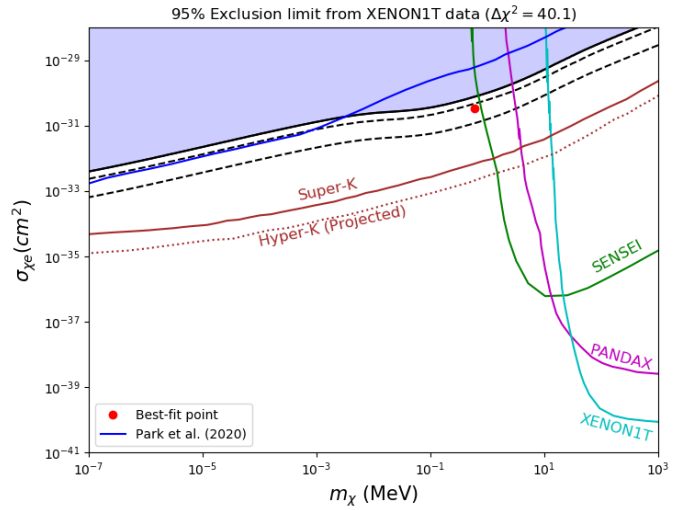


FIG. 5. Blue shaded exclusion region in the $(m_\chi, \sigma_{\chi e})$ plane derived from the XENON1T data at the 95% confidence level for CRE boosted DM assuming $\sigma_{\chi\nu} = 0$. The region between the two dashed lines satisfy $\Delta\chi^2 < 0$, with the best-fit point $(0.6 \text{ MeV}, 3.4 \times 10^{-31} \text{ cm}^2)$ marked as a red point correspond to $\Delta\chi^2 = -4.1$. The constraints from other experiments on light cold DM such as SENSEI [66], PANDAX II [67], XENON1T [68] and the results from Ref. [42] and Ref. [39] for CRE boosted DM derived from XENON1T and Super-K (also Hyper-K projection) data respectively, are shown for comparison.

$\Delta\chi^2 = -3.1$. The constraints from various experiments searching for light cold DM such as SENSEI [66], PANDAX II [67], XENON1T [68] are also shown for comparison. The results of Ref. [42] and Ref. [39], which derive limits on CRE boosted DM from XENON1T and Super-K data respectively, are also given.

Further, we explore the scenario where $\sigma_{\chi\nu, \chi e} \neq 0$ and assume the flux of DSNB neutrinos is the sole contributor to the DM boost i.e., $B = 0$ in Eq.(15). To do this, we repeat the above analysis and obtain a bound on $\sqrt{\sigma_{\chi\nu}\sigma_{\chi e}}$ as a function of DM mass. The results are shown in Fig. 6 and we compare these with the results of Ref. [48] which is analogous to the considered case and of Ref. [47] in which stellar neutrinos instead of DSNB neutrinos, boost the DM. Note that our results are consistent with Ref. [48] for large m_χ values.

As we mentioned earlier, the flux of DSNB neutrinos is comparable to the flux of CRE in that energy range which provides visible recoil energy due to light DM scattering off electron. Therefore, next, we consider contribution of both the fluxes. We assume $\sigma_{\chi\nu} = \sigma_{\chi e}$ and derive the exclusion region, presented in Fig. 7.

Note that the exclusion region in Fig. 5 and Fig. 6 is derived from A and B term of Eq. 15 respectively. In the current case, both terms are combined to set the exclusion limit. For lighter m_χ , A term wins over B , shown in Fig. 14. Thus, the numbers in Fig. 6 and Fig. 7 are similar.

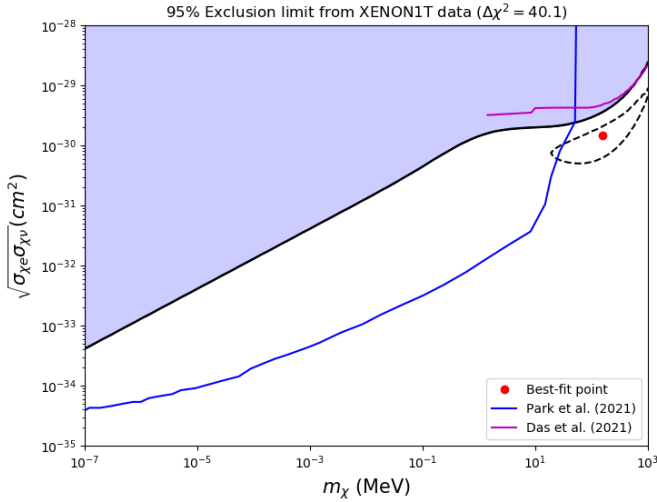


FIG. 6. Exclusion region in the $(m_\chi, \sigma_{\chi e})$ plane derived from the XENON1T data at the 95% confidence level for DSNB boosted DM assuming $B = 0$ in Eq. 15. The region between the dashed contour satisfy $\Delta\chi^2 < 0$, with the best-fit point (156 MeV, $1.5 \times 10^{-30} \text{ cm}^2$) marked as a red point correspond to $\Delta\chi^2 = -3.1$. The constraints based on the results from Ref. [47] for stellar neutrino BDM and Ref. [48] for DSNB BDM, derived from XENON1T data, are shown for comparison.

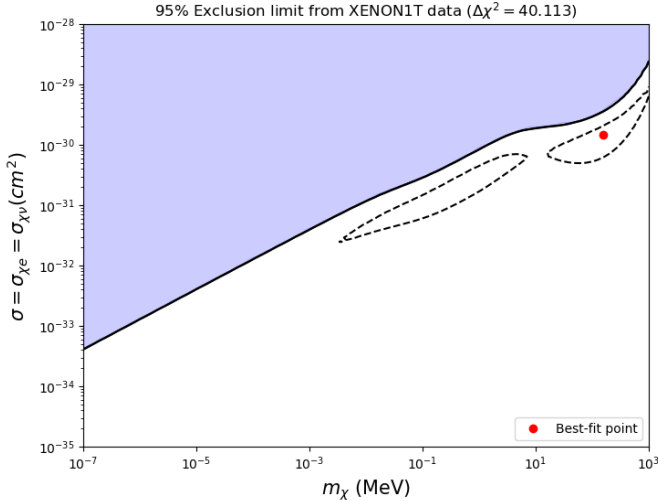


FIG. 7. Exclusion region in the $(m_\chi, \sigma_{\chi\nu} = \sigma_{\chi e})$ plane derived from the XENON1T data at the 95% confidence level for DM boosted by both CRE and DSNB, corresponding to $A \neq 0$ and $B \neq 0$ in Eq. (15). For all points inside the dashed line $\Delta\chi^2 < 0$ and the best fit point (156 MeV, $1.5 \times 10^{-30} \text{ cm}^2$) marked with red point correspond to $\Delta\chi^2 = -3.1$.

We also present the exclusion contours in $\sigma_{\chi\nu} - \sigma_{\chi e}$ plane for different values of m_χ in Fig. 8. The region above the lines is excluded at the 95% confidence level. In the regime $\sigma_{\chi\nu} \gg \sigma_{\chi e}$, the first term in Eq. 15 dominates which implies $\sigma_{\chi e} \sigma_{\chi\nu} = \text{constant}$ and thus is the nature of the curve. For $\sigma_{\chi e} \gg \sigma_{\chi\nu}$, the second term in Eq. 15

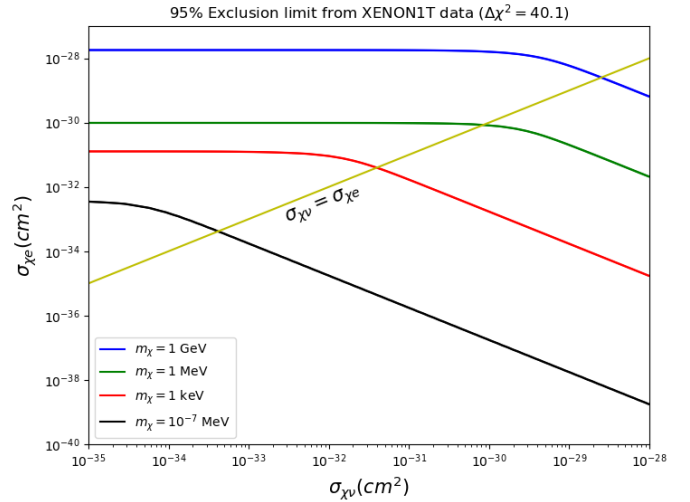


FIG. 8. Exclusion contours in $(\sigma_{\chi\nu}, \sigma_{\chi e})$ plane derived from the XENON1T data for DM boosted by both CRE and DSNB are shown for different values of m_χ . The regions above the solid lines are excluded at the 95% confidence level.

dominates and we obtain a contour independent of $\sigma_{\chi\nu}$. Also, area excluded increases with decreasing DM mass because lighter DM is boosted more and hence it is more constrained.

Super Kamiokande

Super-K is a 50 kiloton water Cherenkov detector build at the Kamioka mine in Japan. The data used for this analysis is referred to as the SK-I data, which was taken for total 1497 days of live-time. The detector directly looks for the DSNB events via inverse beta decay $\bar{\nu}_e + p \rightarrow n + e^+$. In the present work, we assume that the observed events are consistent with the background and hence the signal due to DM should be consistent with the data within the uncertainty. Since an estimate of the background is not found in the literature (to our knowledge), we take $\chi^2(B_0 \text{ only}) = 0$ for SK-I data. In Fig. 9, we have shown the SK-I data along with the predicted no. of events for CRE + DSNB boosted DM for different values of m_χ . Also shown are BDM-induced recoil spectra for different values of $\sigma_{\chi e}$ for $m_\chi = 20 \text{ MeV}$.

We follow the χ^2 analysis similar to XENON1T case to obtain the constraints on the (m_χ, σ) parameter space. We, first, consider the scenario when $\sigma_{\chi\nu} = 0$ and present the results in Fig. 10. Here, the excluded region satisfies $\Delta\chi^2 > 26.3$ which corresponds to 95% exclusion limit for 16 degrees of freedom. As it is evident from Fig. 10, our results agree very well with that of Ref. [39].

In Fig. 11, we show the exclusion region assuming $B = 0$ in Eq. (15) or the flux of DSNB neutrinos is the only contributor to the DM boost. To best of our knowledge, there is no previous study where the exclusion limits on $\sigma_{\chi\nu}$ are derived using SK-I data. Also, these bounds

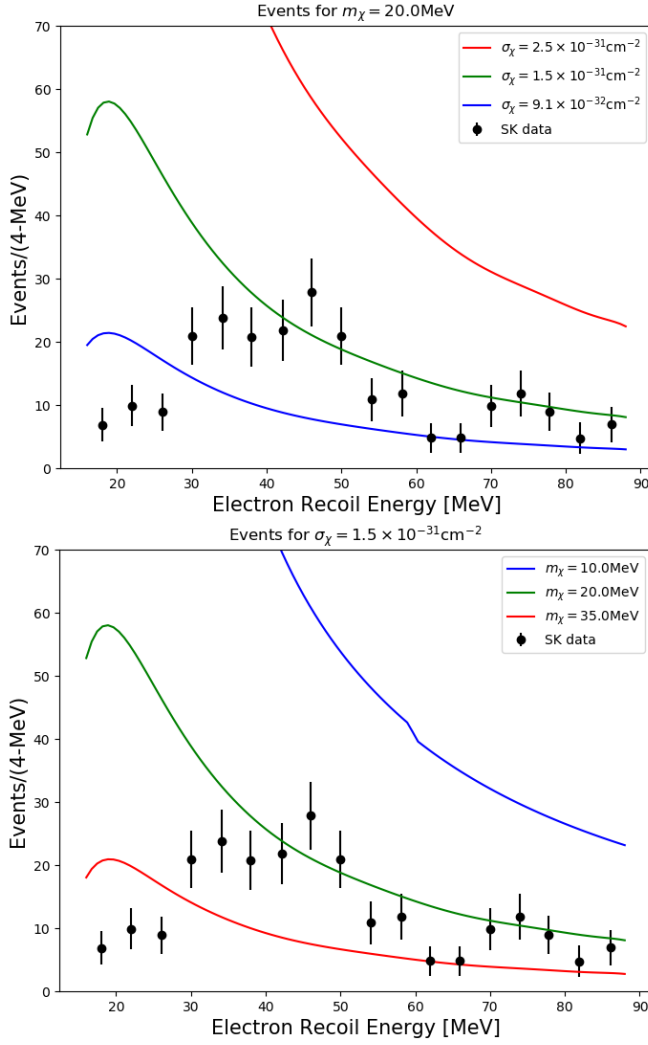


FIG. 9. Super-Kamiokande data [49] along with the predicted no. of events for DM boosted via CRe and DSNB neutrinos. In the upper panel, the no. of events are shown as a function of the electron recoil energy for different values of cross-section at fixed $m_\chi = 20$ MeV. In the bottom panel, the event rate as a function of the recoil energy is given for different values of m_χ at fixed $\sigma = 1.5 \times 10^{-31} \text{cm}^2$. The visible wiggles are present due to the detector efficiency.

are stronger than those obtained in earlier studies for different detectors.

It should be noticed that the exclusion region extends beyond 1 GeV in Fig. 10 which correspond to the CRe boosted DM scenario whereas it is limited to 10 MeV in the case of DSNB boosted DM (Fig. 11). This owes to the fact that DSNB flux decline very rapidly for $T_\nu > 50$ MeV whereas cosmic electron spectra is comparatively significant at larger kinetic energy.

Next, we consider the DSNB + CRe flux which boost the DM and derive the most general exclusion limits. Assuming $\sigma_{\chi\nu} = \sigma_{\chi e}$, we present the exclusion regions and contours in Fig. 12 and Fig. 13 respectively. Note that numbers obtained in this case are comparable to

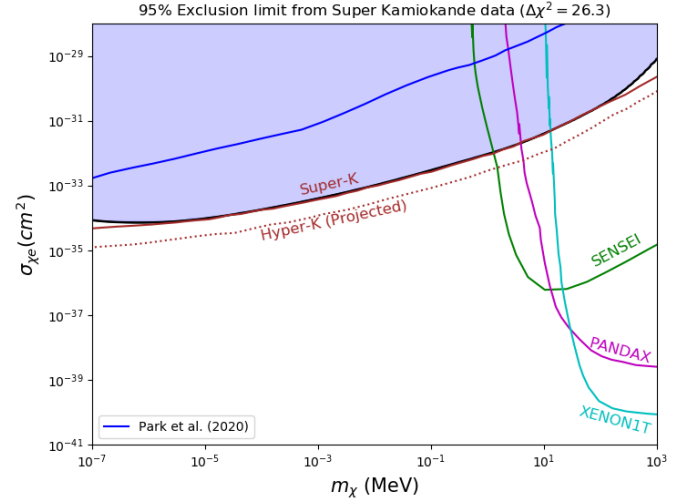


FIG. 10. Exclusion region in the $(m_\chi, \sigma_{\chi e})$ plane derived from the SK I data at the 95% confidence level for CRe boosted DM assuming $\sigma_{\chi\nu} = 0$. The constraints from other experiments on light cold DM such as SENSEI [66], PANDAX II [67], XENON1T [68] and the results from Ref. [39] and Ref. [42] (Park et al.) for CRe boosted DM derived from Super-K (also Hyper-K projection) and XENON1T data respectively, are shown for comparison.

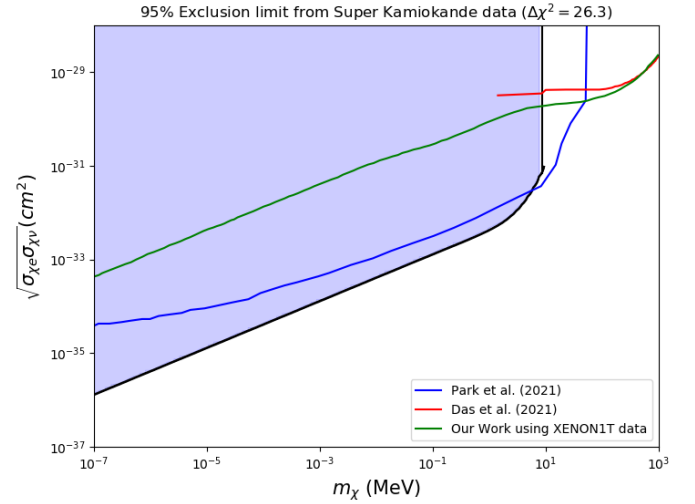


FIG. 11. Exclusion region in the $(m_\chi, \sigma_{\chi e})$ plane derived from the SK I data at the 95% confidence level for DSNB boosted DM assuming $B = 0$ in Eq. 15. The constraints based on the results from Ref. [47] for stellar neutrino BDM and Ref. [48] for DSNB BDM, derived from XENON1T data, are shown for comparison.

that of Fig. 10 for larger masses whereas are similar to DSNB boosted DM case (Fig. 11) for $m_\chi < 10$ MeV. To understand this, we follow Fig. 14 for SK I data. We observe that A term of Eq. 15 dominates over B term for DM of mass less than a few MeV, for $E_R \leq 50$ MeV. Not only it dominates in certain energy range, its magnitude is very large. Therefore, bounds obtained in Fig. 12 for

$m_\chi < 10$ MeV replicates the bounds in Fig. 11.

VI. CONCLUSIONS

In this work, we implemented the idea of boosted DM to set exclusion limits on a combination of DM-electron and DM-neutrino cross-sections for low-mass DM. To register events in the detectors of such DM particle interacting with neutrinos, obviously, we need to assume non-zero interaction strength between DM and the electrons. Therefore we can not ignore the boost due to scattering of DM with CRe while constraining DM-neutrino interactions. Furthermore, we also noted that the flux of the DSNB boosted-DM and the CRe boosted-DM are comparable for light DM in the energy range relevant for XENON1T and Super-Kamiokande. We perform a χ^2 analysis to obtain novel limits in the $(m_\chi, \sigma_{\chi e/\chi\nu})$ plane using XENON1T (a low energy recoil experiment) and Super-K (a high energy recoil experiment) data. We also find the best-fit points explaining the reported excess events by XENON1T collaboration. We systematically study the following cases: (i) cosmic electron boosted DM where only DM-electron interaction is considered, (ii) a scenario where DM particles get boosted only due to their interactions with the neutrinos, and (iii) DM is boosted due to interactions with cosmic electron as well as DSNB. To our knowledge, we are the first to use Super-K data to derive bounds on $\sigma_{\chi\nu}$. We found that Super-Kamiokande, in fact, sets the strongest bound on $\sigma_{\chi\nu}$ for $m_\chi < 10$ MeV, as shown in Fig. 11 and Fig. 12.

We believe that large part of the parameter space for light boosted DM could also be probed with other low-energy recoil experiments like SENSEI [66], CRESST-II [8], PandaX [67] etc., the experiments which usually

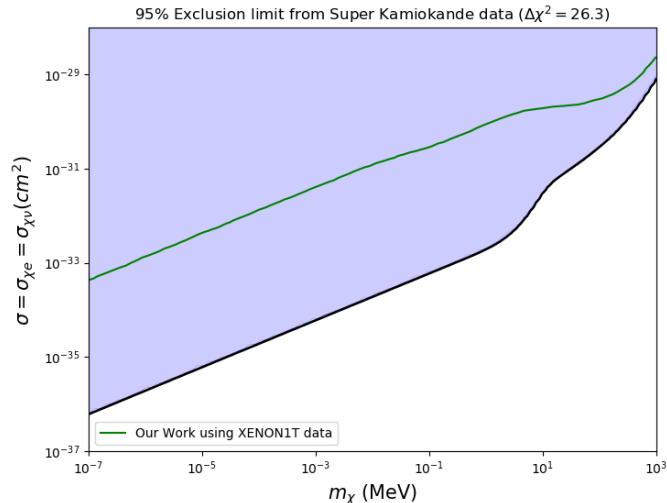


FIG. 12. Exclusion region in the $(m_\chi, \sigma_{\chi\nu} = \sigma_{\chi e})$ plane derived from the SK I data at the 95% confidence level for DM boosted by both CRe and DSNB, corresponding to $A \neq 0$ and $B \neq 0$ in Eq. (15).

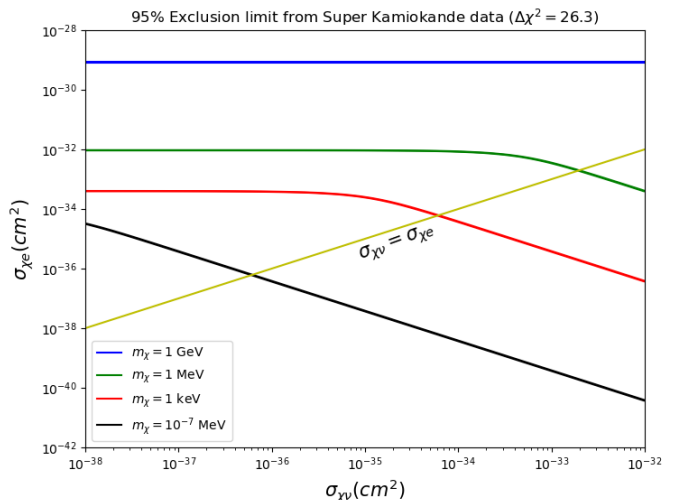


FIG. 13. Exclusion contours in $(\sigma_{\chi\nu}, \sigma_{\chi e})$ plane derived from the SK I data for DM boosted by both CRe and DSNB are shown for different values of m_χ . The regions above the solid lines are excluded at the 95% confidence level.

probe cold DM. Similarly, it would be interesting to see how other neutrino experiments/detectors like Borexino [69], DUNE [70], JUNO [71], Hyper-Kamiokande [72], MiniBooNE [73] could be utilized to rule out the models of boosted DM.

ACKNOWLEDGMENTS

DG and DS acknowledge support through the Ramanujan Fellowship and MATRICS Grant of the Department of Science and Technology, Government of India. DG and AG would like to thank Arun Thalappillil for discussions at the early stage of the work.

Appendix A: Parametric Variation of A and B

In Fig. 14, the coefficients A and B of Eq. 15 have been plotted as a function of the recoil energy for three different DM masses, $m_\chi = 1 \text{ keV}$, 1 MeV , and 1 GeV for both the experiments, XENON1T (left panel) and Super-Kamiokande (right panel). In Fig. 15, on the other hand, variations in A and B are shown as a function of the DM mass for three different recoil energies.

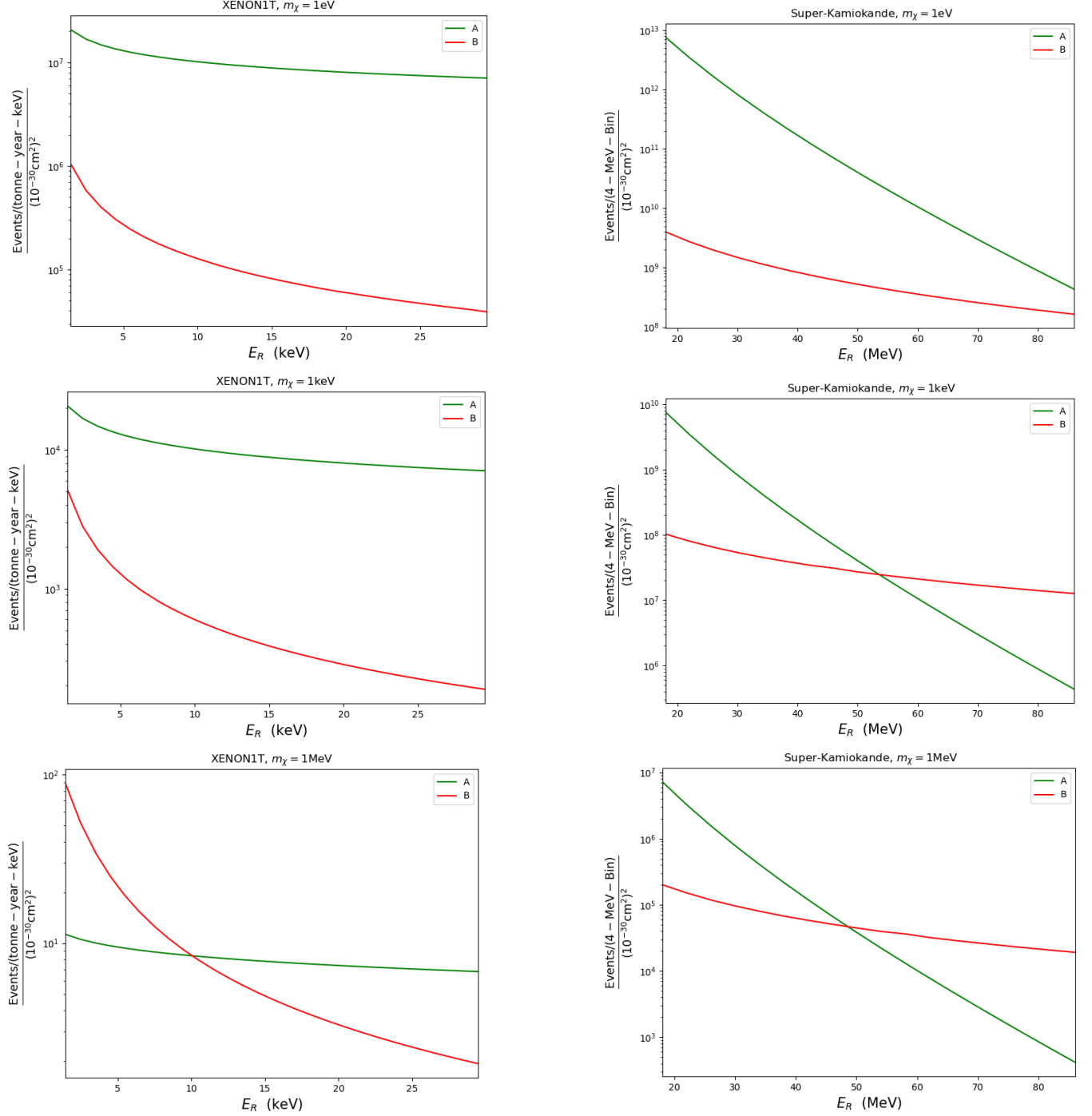


FIG. 14. Variations of A and B as a function of the recoil energy for $m_\chi = 1 \text{ eV}$ (top), $m_\chi = 1 \text{ keV}$ (middle), and $m_\chi = 1 \text{ MeV}$ (bottom). The left panel corresponds to the XENON1T experiment and the right panel corresponds to the Super-Kamiokande experiment.

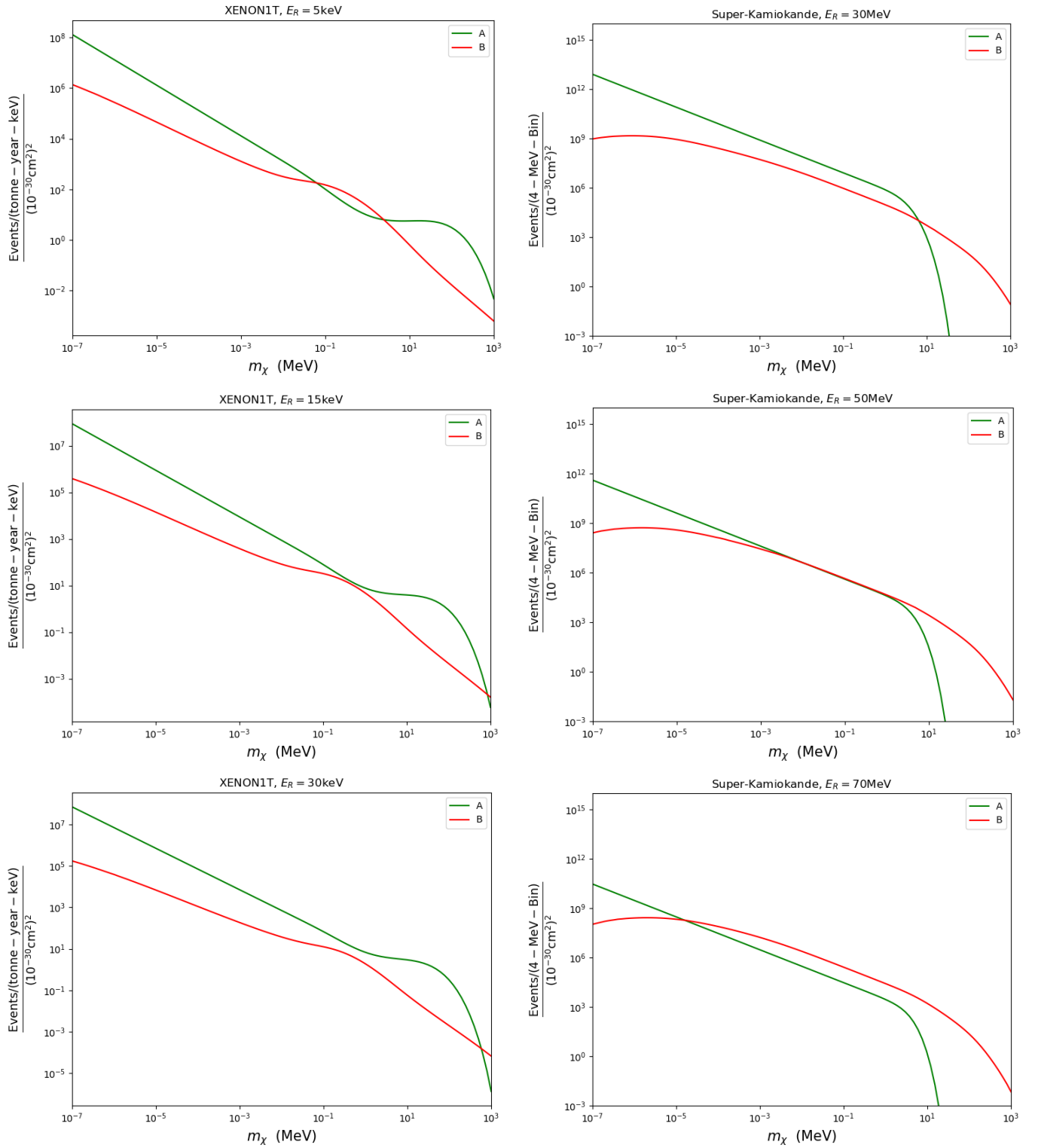


FIG. 15. Variation of A and B for XENON1T(left) and Super-Kamiokande(right) for different recoil energies.

- [1] M. Bauer and T. Plehn, *Yet Another Introduction to Dark Matter: The Particle Physics Approach*, Lecture Notes in Physics, Vol. 959 (Springer, 2019) arXiv:1705.01987 [hep-ph].
- [2] G. Bertone, D. Hooper, and J. Silk, *Phys. Rept.* **405**, 279 (2005), arXiv:hep-ph/0404175.
- [3] M. Lisanti, in *Theoretical Advanced Study Institute in Elementary Particle Physics: New Frontiers in Fields and Strings* (2017) pp. 399–446, arXiv:1603.03797 [hep-ph].
- [4] S. Profumo, in *Theoretical Advanced Study Institute in Elementary Particle Physics: Searching for New Physics at Small and Large Scales* (2013) pp. 143–189, arXiv:1301.0952 [hep-ph].
- [5] E. Aprile *et al.* (XENON), *Eur. Phys. J. C* **80**, 785 (2020), arXiv:2003.03825 [physics.ins-det].
- [6] E. Aprile *et al.* (XENON), *Phys. Rev. D* **102**, 072004 (2020), arXiv:2006.09721 [hep-ex].
- [7] M. Crisler, R. Essig, J. Estrada, G. Fernandez, J. Tiffenberg, M. Sofo haro, T. Volansky, and T.-T. Yu (SENSEI), *Phys. Rev. Lett.* **121**, 061803 (2018), arXiv:1804.00088 [hep-ex].
- [8] G. Angloher *et al.* (CRESSST), *Eur. Phys. J. C* **76**, 25 (2016), arXiv:1509.01515 [astro-ph.CO].
- [9] P. Agnes *et al.* (DarkSide), *Phys. Rev. Lett.* **121**, 111303 (2018), arXiv:1802.06998 [astro-ph.CO].
- [10] E. Aprile *et al.* (XENON), *JCAP* **04**, 027 (2016), arXiv:1512.07501 [physics.ins-det].
- [11] R. Essig, A. Manalaysay, J. Mardon, P. Sorensen, and T. Volansky, *Phys. Rev. Lett.* **109**, 021301 (2012), arXiv:1206.2644 [astro-ph.CO].
- [12] O. Abramoff *et al.* (SENSEI), *Phys. Rev. Lett.* **122**, 161801 (2019), arXiv:1901.10478 [hep-ex].
- [13] M. Baryakhtar, J. Bramante, S. W. Li, T. Linden, and N. Raj, *Phys. Rev. Lett.* **119**, 131801 (2017), arXiv:1704.01577 [hep-ph].
- [14] B. Dasgupta, A. Gupta, and A. Ray, *JCAP* **08**, 018 (2019), arXiv:1906.04204 [hep-ph].
- [15] D. Bose, T. N. Maity, and T. S. Ray, (2021), arXiv:2108.12420 [hep-ph].
- [16] A. Guha and D. Sen, *JCAP* **09**, 027 (2021), arXiv:2106.10353 [hep-ph].
- [17] D. Sen and A. Guha, *Mon. Not. Roy. Astron. Soc.* **504**, 3 (2021), arXiv:2104.06141 [hep-ph].
- [18] J. F. Acevedo, J. Bramante, A. Goodman, J. Kopp, and T. Opferkuch, *JCAP* **04**, 026 (2021), arXiv:2012.09176 [hep-ph].
- [19] R. K. Leane and J. Smirnov, *Phys. Rev. Lett.* **126**, 161101 (2021), arXiv:2010.00015 [hep-ph].
- [20] R. Garani, A. Gupta, and N. Raj, *Phys. Rev. D* **103**, 043019 (2021), arXiv:2009.10728 [hep-ph].
- [21] A. Joglekar, N. Raj, P. Tanedo, and H.-B. Yu, *Phys. Rev. D* **102**, 123002 (2020), arXiv:2004.09539 [hep-ph].
- [22] A. Joglekar, N. Raj, P. Tanedo, and H.-B. Yu, *Phys. Lett. B*, 135767 (2020), arXiv:1911.13293 [hep-ph].
- [23] D. Green and S. Rajendran, *JHEP* **10**, 013 (2017), arXiv:1701.08750 [hep-ph].
- [24] D. Baumann, D. Green, and B. Wallisch, *Phys. Rev. Lett.* **117**, 171301 (2016), arXiv:1604.08614 [astro-ph.CO].
- [25] G. Krnjaic and S. D. McDermott, *Phys. Rev. D* **101**, 123022 (2020), arXiv:1908.00007 [hep-ph].
- [26] D. McKeen, M. Pospelov, and N. Raj, *Phys. Rev. Lett.* **125**, 231803 (2020), arXiv:2006.15140 [hep-ph].
- [27] G. G. Raffelt, *Lect. Notes Phys.* **741**, 51 (2008), arXiv:hep-ph/0611350.
- [28] G. G. Raffelt, *Ann. Rev. Nucl. Part. Sci.* **49**, 163 (1999), arXiv:hep-ph/9903472.
- [29] K. Kadota and J. Silk, *Phys. Rev. D* **89**, 103528 (2014), arXiv:1402.7295 [hep-ph].
- [30] H. K. Dreiner, J.-F. Fortin, C. Hanhart, and L. Ubaldi, *Phys. Rev. D* **89**, 105015 (2014), arXiv:1310.3826 [hep-ph].
- [31] A. Guha, P. S. B. Dev, and P. K. Das, *JCAP* **02**, 032 (2019), arXiv:1810.00399 [hep-ph].
- [32] Y. Bai and A. Rajaraman, (2011), arXiv:1109.6009 [hep-ph].
- [33] T. Cohen, M. Lisanti, and H. K. Lou, *Phys. Rev. Lett.* **115**, 171804 (2015), arXiv:1503.00009 [hep-ph].
- [34] Y. Ali-Haïmoud, *Phys. Rev. D* **103**, 043541 (2021), arXiv:2101.04070 [astro-ph.CO].
- [35] D. Nguyen, D. Sarnaik, K. K. Boddy, E. O. Nadler, and V. Gluscevic, (2021), arXiv:2107.12380 [astro-ph.CO].
- [36] R. J. Wilkinson, C. Boehm, and J. Lesgourgues, *JCAP* **05**, 011 (2014), arXiv:1401.7597 [astro-ph.CO].
- [37] T. Bringmann and M. Pospelov, *Phys. Rev. Lett.* **122**, 171801 (2019), arXiv:1810.10543 [hep-ph].
- [38] C. V. Cappiello, K. C. Y. Ng, and J. F. Beacom, *Phys. Rev. D* **99**, 063004 (2019), arXiv:1810.07705 [hep-ph].
- [39] C. V. Cappiello and J. F. Beacom, *Phys. Rev. D* **100**, 103011 (2019), [Erratum: *Phys.Rev.D* 104, 069901 (2021)], arXiv:1906.11283 [hep-ph].
- [40] Y. Ema, F. Sala, and R. Sato, *Phys. Rev. Lett.* **122**, 181802 (2019), arXiv:1811.00520 [hep-ph].
- [41] J. B. Dent, B. Dutta, J. L. Newstead, I. M. Shoemaker, and N. T. Arellano, *Phys. Rev. D* **103**, 095015 (2021), arXiv:2010.09749 [hep-ph].
- [42] Y. Jho, J.-C. Park, S. C. Park, and P.-Y. Tseng, *Phys. Lett. B* **811**, 135863 (2020), arXiv:2006.13910 [hep-ph].
- [43] J. Bramante, B. J. Kavanagh, and N. Raj, (2021), arXiv:2109.04582 [hep-ph].
- [44] Y. Farzan and S. Palomares-Ruiz, *JCAP* **06**, 014 (2014), arXiv:1401.7019 [hep-ph].
- [45] C. A. Argüelles, A. Kheirandish, and A. C. Vincent, *Phys. Rev. Lett.* **119**, 201801 (2017), arXiv:1703.00451 [hep-ph].
- [46] W. Yin, *EPJ Web Conf.* **208**, 04003 (2019), arXiv:1809.08610 [hep-ph].
- [47] Y. Jho, J.-C. Park, S. C. Park, and P.-Y. Tseng, (2021), arXiv:2101.11262 [hep-ph].
- [48] A. Das and M. Sen, (2021), arXiv:2104.00027 [hep-ph].
- [49] K. Bays *et al.* (Super-Kamiokande), *Phys. Rev. D* **85**, 052007 (2012), arXiv:1111.5031 [hep-ex].
- [50] M. J. Boschini *et al.*, *Astrophys. J.* **854**, 94 (2018), arXiv:1801.04059 [astro-ph.HE].
- [51] M. Ackermann *et al.* (Fermi-LAT), *Phys. Rev. Lett.* **108**, 011103 (2012), arXiv:1109.0521 [astro-ph.HE].
- [52] A. A. Abdo *et al.* (Fermi-LAT), *Phys. Rev. Lett.* **102**, 181101 (2009), arXiv:0905.0025 [astro-ph.HE].
- [53] M. Ackermann *et al.* (Fermi-LAT), *Phys. Rev. D* **82**, 092004 (2010), arXiv:1008.3999 [astro-ph.HE].
- [54] S. Abdollahi *et al.* (Fermi-LAT), *Phys. Rev. D* **95**, 082007 (2017), arXiv:1704.07195 [astro-ph.HE].

- [55] M. Aguilar *et al.* (AMS), *Phys. Rev. Lett.* **113**, 221102 (2014).
- [56] O. Adriani *et al.* (PAMELA), *Phys. Rev. Lett.* **106**, 201101 (2011), [arXiv:1103.2880 \[astro-ph.HE\]](#).
- [57] O. Adriani *et al.* (CALET), *Phys. Rev. Lett.* **119**, 181101 (2017), [arXiv:1712.01711 \[astro-ph.HE\]](#).
- [58] A. C. Cummings, E. C. Stone, B. C. Heikkila, N. Lal, W. R. Webber, G. Jóhannesson, I. V. Moskalenko, E. Orlando, and T. A. Porter, *Astrophys. J.* **831**, 18 (2016).
- [59] E. C. Stone, A. C. Cummings, F. B. McDonald, B. C. Heikkila, N. Lal, and W. R. Webber, *Science* **341**, 150 (2013).
- [60] J. F. Beacom, *Ann. Rev. Nucl. Part. Sci.* **60**, 439 (2010), [arXiv:1004.3311 \[astro-ph.HE\]](#).
- [61] S. Horiuchi, J. F. Beacom, and E. Dwek, *Phys. Rev. D* **79**, 083013 (2009), [arXiv:0812.3157 \[astro-ph\]](#).
- [62] C. Lunardini, *Astropart. Phys.* **79**, 49 (2016), [arXiv:1007.3252 \[astro-ph.CO\]](#).
- [63] H. Zhang *et al.* (Super-Kamiokande), *Astropart. Phys.* **60**, 41 (2015), [arXiv:1311.3738 \[hep-ex\]](#).
- [64] N. Aghanim *et al.* (Planck), *Astron. Astrophys.* **641**, A6 (2020), [Erratum: *Astron. Astrophys.* 652, C4 (2021)], [arXiv:1807.06209 \[astro-ph.CO\]](#).
- [65] E. Aprile *et al.* (XENON), *Phys. Rev. Lett.* **121**, 111302 (2018), [arXiv:1805.12562 \[astro-ph.CO\]](#).
- [66] L. Barak *et al.* (SENSEI), *Phys. Rev. Lett.* **125**, 171802 (2020), [arXiv:2004.11378 \[astro-ph.CO\]](#).
- [67] C. Cheng *et al.* (PandaX-II), *Phys. Rev. Lett.* **126**, 211803 (2021), [arXiv:2101.07479 \[hep-ex\]](#).
- [68] E. Aprile *et al.* (XENON), *Phys. Rev. Lett.* **123**, 251801 (2019), [arXiv:1907.11485 \[hep-ex\]](#).
- [69] G. Bellini *et al.*, *Phys. Rev. Lett.* **107**, 141302 (2011), [arXiv:1104.1816 \[hep-ex\]](#).
- [70] R. Acciarri *et al.* (DUNE), (2015), [arXiv:1512.06148 \[physics.ins-det\]](#).
- [71] F. An *et al.* (JUNO), *J. Phys. G* **43**, 030401 (2016), [arXiv:1507.05613 \[physics.ins-det\]](#).
- [72] K. Abe *et al.* (Hyper-Kamiokande), *PTEP* **2018**, 063C01 (2018), [arXiv:1611.06118 \[hep-ex\]](#).
- [73] A. A. Aguilar-Arevalo *et al.* (MiniBooNE DM), *Phys. Rev. D* **98**, 112004 (2018), [arXiv:1807.06137 \[hep-ex\]](#).